



Research article

Molecular interactions of tannic acid and matrix metalloproteinases 2 and 9

Ya-Tang Chiang ^{a,1}, Yu-Bai Xiao ^{b,1}, Shan-hui Hsu ^{a,*}, Shu-Wei Chang ^{b,c,**}, Chia-Ching Chou ^{d,*}^a Institute of Polymer Science and Engineering, National Taiwan University, Roosevelt Road No. 1, Section 4, 10617 Taipei, Taiwan^b Department of Civil Engineering, College of Engineering, National Taiwan University, Roosevelt Road No. 1, Section 4, 10617 Taipei, Taiwan^c Department of Biomedical Engineering, College of Engineering, National Taiwan University, Roosevelt Road No. 1, Section 4, 10617 Taipei, Taiwan^d Institute of Applied Mechanics, College of Engineering, National Taiwan University, Roosevelt Road No. 1, Section 4, 10617 Taipei, Taiwan

ARTICLE INFO

Article history:

Received 8 November 2022

Received in revised form 13 April 2023

Accepted 13 April 2023

Available online 14 April 2023

Keywords:

Hydrogel

Tannic acid

Matrix metalloproteinase 2

Matrix metalloproteinase 9

Molecular docking

ABSTRACT

Tannic acid (TA) has antibacterial, antioxidant, and anti-inflammatory properties and acts as an adhesive, hemostatic, and crosslinking agent in hydrogels. Matrix metalloproteinases (MMPs), a family of endopeptidase enzymes, play important roles in tissue remodeling and wound healing. TA has been reported to inhibit MMP-2/-9 activities, thereby improving both tissue remodeling and wound healing. However, the mechanism of interaction of TA with MMP-2 and MMP-9 has not been fully elucidated. In this study, the full atomistic modeling approach was applied to explore the mechanisms and structures of TA binding with MMP-2 and MMP-9. Macromolecular models of the TA-MMP-2/-9 complex were built by docking based on experimentally resolved MMP structures, and further equilibrium processes were examined by molecular dynamics (MD) simulations to investigate the binding mechanism and structural dynamics of the TA-MMP-2/-9 complexes. The molecular interactions between TA and MMPs, including H-bond formation and hydrophobic and electrostatic interactions, were analyzed and decoupled to elucidate the dominant factors in TA-MMP binding. TA binds to MMPs mainly at two binding regions, residues 163–164 and 220–223 in MMP-2 and residues 179–190 and 228–248 in MMP-9. Two arms of TA participate in binding MMP-2 with 3.61 hydrogen bonds. On the other hand, TA binds MMP-9 with a distinct configuration involving four arms with 4.75 hydrogen bonds, resulting in a tighter binding conformation. Understanding the binding mechanism and structural dynamics of TA with these two MMPs provides crucial and fundamental knowledge regarding the inhibitory and stabilizing effects of TA on MMPs.

© 2023 The Authors. Published by Elsevier B.V. on behalf of Research Network of Computational and Structural Biotechnology. This is an open access article under the CC BY-NC-ND license (<http://creativecommons.org/licenses/by-nc-nd/4.0/>).

1. Introduction

Hydrogels are water-swollen, cross-linked three-dimensional polymer networks [1–4]. They are promising biomaterials for biomedical applications, such as drug delivery, wound dressing, tissue engineering, and bioadhesives [1,4–7]. They exhibit desirable properties, such as forming different shapes, providing a moist environment, absorbing wound exudate, and preventing bacterial growth [8,9]. Traditional hydrogels have the disadvantages of weak

mechanical properties and limited functions. Among hydrogel-forming materials, tannic acid (TA) is a natural, hydrolyzable, plant-derived polyphenol compound with antibacterial, antioxidant, and anti-inflammatory properties [10–13]. As a natural cross-linking agent within biomaterials, it is used in dentine pretreatment to reduce the denaturation and perturbation of collagen [14,15]. TA is also applied to improve the mechanical properties of the dentin matrix [16,17]. Recently, there has been research on the ability of surface modification with TA to enhance biomineralization at the collagen-mineral interface [18]. In addition to its application in dentistry, TA can improve the mechanical properties of natural and synthetic hydrogels and act as an adhesive and hemostatic agent [10]. Because of these excellent properties, tannic acid plays an important role in multifunctional hydrogels for wound healing treatment [8]. The chemical structure of TA consists of a glucose unit center surrounded by ten gallic acid (GA) fragments [11]. It contains polyphenol

* Corresponding authors.

** Corresponding author at: Department of Civil Engineering, College of Engineering, National Taiwan University, Roosevelt Road No. 1, Section 4, 10617 Taipei, Taiwan.

E-mail addresses: shhsu@ntu.edu.tw (S.-h. Hsu),changsw@ntu.edu.tw (S.-W. Chang), ccchou@iam.ntu.edu.tw (C.-C. Chou).¹ Contributed equally to this work.

functional groups that enable a variety of supramolecular interactions with other biomolecules, such as hydrogen bonding and metal–organic coordination bonds [12]. In addition, the benzene ring structure in TA enables hydrophobic interactions with proteins [19].

Matrix metalloproteinases (MMPs) are a family of endopeptidase enzymes with parallel sequence homology and sequence structure [20] that are expressed in physiological and pathological conditions involving inflammation [21]. Because their function is to cleave extracellular matrix (ECM) proteins, they play important roles in tissue remodeling [20,22]. Twenty-three types of MMPs have been identified in humans thus far. Based on their substrates, MMPs can be classified into collagenases, gelatinases, stromelysins, matrilysins, membrane-type MMPs and other MMPs [23]. After injury, the temporal and spatial regulation of MMPs is important for fast and normal wound healing. When the balance between MMPs and tissue inhibitors of metalloproteinases (TIMPs) is disrupted, excess MMPs interfere with matrix remodeling and prevent cell migration, and chronic or nonhealing ulcers may develop. Compared to normal wounds, chronic wounds contain significantly elevated concentrations of MMPs, such as MMP-2 and MMP-9 [24,25]. Thus, to improve chronic wound healing, it is important to control MMP activity [24]. The expression of MMP-2 and MMP-9 in physiological processes is also associated with many human diseases, such as cardiovascular disease, neurodegenerative disease, diabetes mellitus, gynecologic disease, and obstetric disease [25,26].

Recent literature has described the effectiveness of TA hydrogels for wound healing because of their antioxidative properties [13,27–29]. Previous studies have also reported that phenolic compounds may inhibit the activity of proteolytic enzymes [19]. In addition, gelatin zymography experiments have shown that TA can inhibit MMP-2 and MMP-9 activity [30]. However, few of these literature reports have discussed the mechanism of interaction of TA with MMP-2 and MMP-9 due to the difficulty of experimental operation and observation. Compared to the *in vitro* method, the *in silico* method benefits from high spatial and temporal resolution and further provides insights into the molecular interactions between TA and MMP-2 and MMP-9.

In this study, a full atomistic modeling approach, including molecular docking and molecular dynamics simulation, was applied to study the interaction mechanism of TA with MMP-2 and MMP-9 at the atomic scale. We explored the mechanism and structural dynamics of the binding of TA with MMP-2 and MMP-9 and shed new light on opportunities to use this new multifunctional hydrogel design for tissue remodeling and wound healing.

2. Methods

2.1. Molecular structures of MMPs and TA

The structures of TA, MMP-2, and MMP-9 are shown in Fig. 1. TA (Fig. 1a) is a star-shaped polymer with five digallic acid arms [31]. One TA molecule contains five pyrogallol groups in exterior positions and five catechol groups in interior positions [6]. The TA molecular structure (Molid 721259) optimized by the quantum mechanics method was obtained from Automated Topology Builder [32]. The TA molecular structure is shown in Fig. 1(b). Fig. 1(c) and (d) show the X-ray crystallography structures of MMP-2 (PDB ID: 1QJB) [33] and MMP-9 (PDB ID: 5I12) [34] from the RCSB Protein Data Bank (PDB). Both secondary structures are labeled according to the PDB files. MMP-2 and MMP-9 contain three alpha helices (hA, hB, and hC) and five beta strands (sI, sII, sIII, sIV, and sV). Common loops are named according to the neighboring secondary structures, for instance, the loop between sI and hA is labeled as LsI-hA. One of two zinc ions is the catalytic zinc ion (Zn501 for MMP-2 and Zn301 for MMP-9)

[33,34]. The main sequence differences between the catalytic domains of MMP-2 and MMP-9 are S1' specificity loops that form the S1' pocket [35].

2.2. Molecular docking simulations

Molecular docking simulations were performed using AutoDock Vina 1.1.2 [36]. The two-step approach, the blind docking procedure and the pocket search method were described in a previous study [37]. The PDB files of TA, MMP-2, and MMP-9 were converted to PDBQT files by AutoDockTool 1.5.7 [38]. For TA, Gasteiger partial charges were added [39]. For MMP-2 and MMP-9, water and ligands were removed [40], polar hydrogens were added, and Kollman charges were assigned [39].

2.3. Molecular dynamics simulations

The pocket search results with the strongest binding affinity were selected as the initial structures for molecular dynamics simulations. These two models were called the TA–MMP-2 and TA–MMP-9 complexes. Two additional models without TA were called Free MMP-2 and Free MMP-9. Molecular dynamics (MD) simulations were performed with NAMD 2.12 [41] software using CHARMM36 force fields [42]. The topology of the TA was generated using a CHARMM-GUI ligand reader and modeler [43]. Each model was solvated in a cubic box with a side length of 90 Å and neutralized with 0.15 M NaCl by the VMD plugin. The models were energy minimized and equilibrated for 100 ns at 300 K and 1 atm with a time step of 2 fs. The average value and standard deviation of the measurement were calculated for the last 10 ns of the simulation.

2.4. Calculation of molecular interactions

Hydrogen bonds were calculated when the distance between the donor and acceptor was less than 3.5 Å and the donor–hydrogen–acceptor angle was less than 30 degrees [44,45]. Metal–organic coordination bonds between catalytic zinc ions and oxygen atoms of TA were calculated when the bond distance was less than 2.7 Å [40].

2.5. The calculation of total nonbonded energy and decomposition of nonbonded energy

The total nonbonded energies and decomposition of nonbonded energies between the two MMPs and TA were calculated according to the nonbonded terms of the potential energy functions of CHARMM force fields [46] using the VMD plugin. The nonbonded energy was decomposed into van der Waals and electrostatic energies. We further categorized the nonbonded energy of residues and ion components in MMPs into three types of interaction: hydrogen bonds, hydrophobic interaction and metal–organic coordination bonding.

3. Results and discussion

3.1. Binding interactions of TA–MMP-2 and TA–MMP-9

The molecular docking binding affinities for the TA–MMP-2 and TA–MMP-9 complexes are -8.2 and -8.6 kcal/mol, respectively, which are both in reasonable ranges for most of the macromolecular docking results [47]. We first analyzed the intermolecular hydrogen bonds between TA and the two MMPs. The number of hydrogen bonds for the TA–MMP-2 and TA–MMP-9 complexes were 3.61 ± 1.09 and 4.75 ± 1.23 , respectively. There were more hydrogen bonds between TA and MMP-9 than between TA and MMP-2,

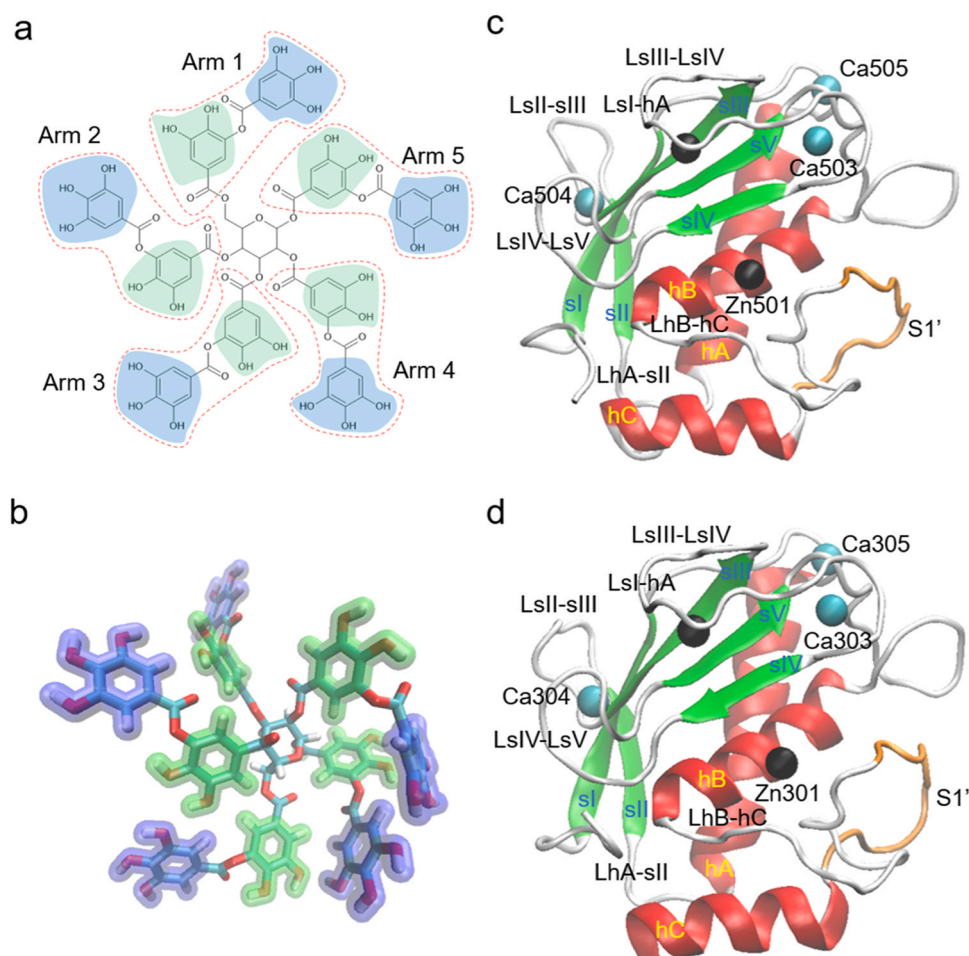


Fig. 1. (a) Chemical structure of TA. The red dotted line represents the boundary between the glucose unit and the digallic acid arm, the blue shade represents the pyrogallol group, and the green shade represents the catechol group. (b) Molecular structure of TA. Carbon, oxygen, and hydrogen are represented by green, red, and white, respectively. (c) Crystal structure of the catalytic domain of MMP-2 (PDB ID: 1QJB). (d) Crystal structure of the catalytic domain of MMP-9 (PDB ID: 5I12). Beta strands, alpha helices, coils, S1' specificity loops, zinc ions, and calcium ions are represented by green, red, white, orange, black, and cyan, respectively.

indicating that the TA–MMP-9 complex had stronger hydrogen bonding interactions than the TA–MMP-2 complex. The detailed analysis of intermolecular hydrogen bonds between the functional groups of the five digallic acid arms of TA and MMP-2 and MMP-9 is shown in Fig. 2(a) and (b). The results showed that two of the five digallic acid arms of TA had more than 0.5 hydrogen bonds with MMP-2, and four of the five digallic acid arms of TA had more than 0.5 hydrogen bonds with MMP-9. These results were consistent with the total number of hydrogen bonds. There were almost no hydrogen bonds between the glucose units of TA and the two MMPs. Both the pyrogallol groups and the catechol groups of TA had the ability to bind with MMP-2 and MMP-9. The number of hydrogen bonds of TA carbonyl or ether groups with the two MMPs was lower. The results indicated that the pyrogallol groups and catechol groups of TA were the major functional groups that formed hydrogen bonds with the two MMPs. Detailed information on the individual intermolecular hydrogen bonds between TA and the two MMPs is also listed in Tables S1 and S2.

Fig. 3 shows the hydrogen bonds and the metal–organic coordination bonds in 2D interaction plots and the equilibrated binding structures in the MD simulation for the TA–MMP-2 complex and the TA–MMP-9 complex. The hydrogen bonds between TA and the two MMPs and the metal–organic coordination bonds between TA and the catalytic zinc ions are highlighted in red and blue, respectively, in the figure. For the hydrogen bonding interaction, the

2D interaction plots in Fig. 3(a) show the corresponding chemical structures of TA and the residues of MMP-2. In Fig. 3(b), the molecular structures of the TA–MMP-2 complex showed that only two arms of TA interacted with MMP-2, and the other arms were stretched away from the MMP-2 molecule. In Fig. 3(c) and (d), TA was bound closely to MMP-9, and the four arms of TA interacted tightly with the residues of MMP-9. We further analyzed the binding sites and the bond distances of metal–organic coordination bonds for catalytic zinc ions. Fig. 3(a) and (b) show that one of the oxygen atoms of TA in the catechol group bound with zinc ions with a bond length of 2.34 ± 0.11 in the TA–MMP-2 complex. Fig. 3(c) and (d) show that one of the oxygen atoms of TA in the carbonyl group bound with zinc ions with a bond length of 2.11 ± 0.07 in the TA–MMP-9 complex. The high occupancy of metal–organic coordination bonds of TA with MMP-2 and MMP-9 indicated stable metal–organic coordination bonds. However, in this study, TA bound with the zinc catalytic ions of two MMPs, indicating that the selectivity between different types of MMPs may not meet the requirements for an ideal selective inhibitor of MMPs [23].

3.2. Total nonbonded and decomposition of nonbonded energy

To understand the binding ability of TA for the two MMPs, the total nonbonded energies and decomposition of nonbonded energies between TA and the two MMPs were calculated. The results showed that

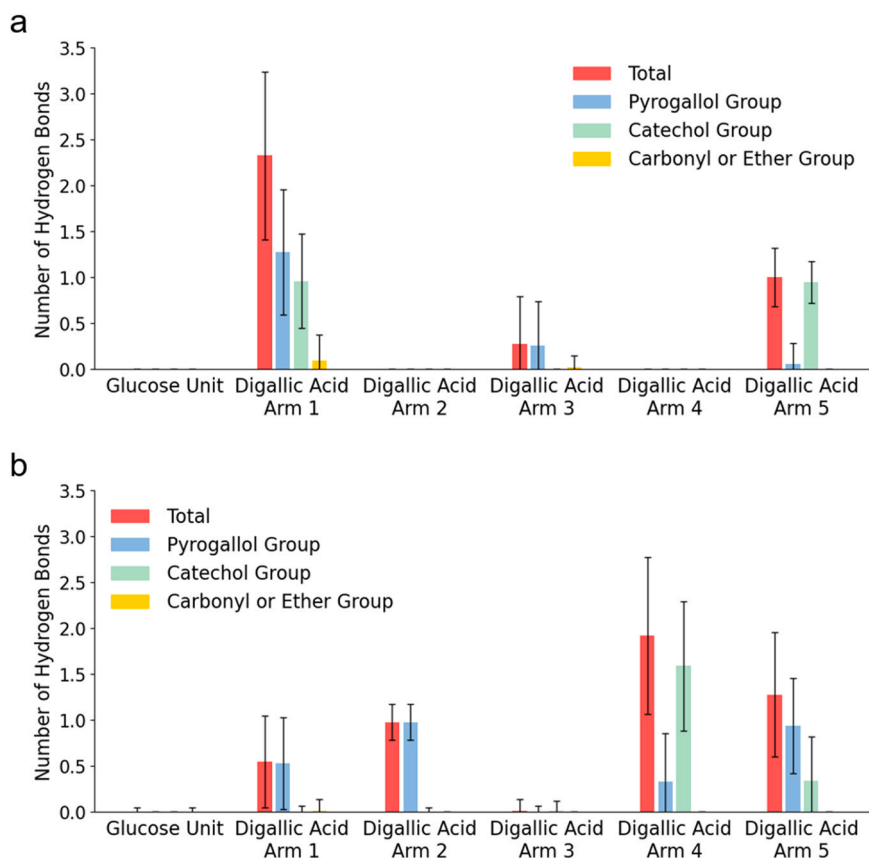


Fig. 2. Detailed analysis of intermolecular hydrogen bonds between glucose units and functional groups of five digallic acid arms of TA and (a) MMP-2 and (b) MMP-9.

the total nonbonded energy for MMP-9 was -182.54 ± 10.53 kcal/mol, which was lower than the energy of -163.96 ± 11.68 kcal/mol for MMP-2, indicating that the binding affinity of TA for MMP-9 was stronger than that for MMP-2. The nonbonded energy was further decomposed into van der Waals and electrostatic energies. The results showed that the electrostatic and van der Waals energies for MMP-2 were -87.94 ± 11.75 kcal/mol and -76.02 ± 4.52 kcal/mol, respectively, and the electrostatic and van der Waals energies for MMP-9 were -98.49 ± 9.74 kcal/mol and -84.04 ± 5.33 , respectively. Both the van der Waals and electrostatic energies for MMP-2 and MMP-9 were strong, indicating that van der Waals and electrostatic energies were both important for binding. The results of the nonbonded energy calculation were consistent with the results of hydrogen bond analysis, showing that the TA-MMP-9 complex had a more stable molecular structure than the TA-MMP-2 complex.

To obtain the detailed contribution of the nonbonded energy, decomposition of the nonbonded energy was carried out to search for key sites in two MMPs. Sites with nonbonded energies lower than -5 kcal/mol were considered important binding sites. Tables S3 and S4 show the detailed decomposition of the nonbonded energy between TA, zinc ions and residues of the two MMPs. The results showed that the nonbonded energy between catalytic zinc ions and TA was -51.26 ± 9.90 and -65.14 ± 9.51 kcal/mol for the TA-MMP-2 and TA-MMP-9 complexes, respectively. The catalytic zinc ions contributed substantially to the nonbonded energy owing to their strong metal-organic coordination bonds. The nonbonded energy contribution of catalytic zinc ions for the TA-MMP-9 complex was larger than that of TA-MMP-2, which was consistent with the total nonbonded energy results. The hydrophobic interactions for the molecular structures of the TA-MMP-2 and TA-MMP-9 complexes

are visualized in Fig. 4. Table S3 shows one ion contributing to metal-organic coordination bonding, three residues contributing to hydrogen bonding, and three residues contributing to hydrophobic interactions in the TA-MMP-2 complex. Table S4 shows one ion contributing to metal-organic coordination bonding, five residues contributing to hydrogen bonding, and seven residues contributing to hydrophobic interactions in the TA-MMP-9 complex. The TA-MMP-9 complex had more residues contributing to hydrogen bonding and hydrophobic interactions than the TA-MMP-2 complex. These results were consistent with the total nonbonded energy calculations. The bar chart representations of Tables S3 and S4 are shown in Fig. 5. The above key sites may provide guidance for rational design to discover potential multifunctional TA hydrogels.

3.3. Structural analysis of the TA-MMP-2 and TA-MMP-9 complexes

To investigate the binding-induced structural changes of the two MMPs, the root mean square deviation (RMSD) and radius of gyration (Rg) for backbone atoms of proteins were calculated during the trajectories of MD simulations. RMSD is the measurement method for comparing the similarity between two superimposed atomic coordinates [48], and Rg is the measurement method for protein compactness [49]. Fig. 6(a) and (b) show the RMSD and Rg results for both free MMPs and both TA-MMP complexes. The RMSD values for the free MMP-2 and the TA-MMP-2 complex were 1.85 ± 0.18 and 1.94 ± 0.15 , respectively, and those for the free MMP-9 and the TA-MMP-9 complex were 1.49 ± 0.11 and 1.80 ± 0.08 , respectively. The Rg values for the free MMP-2 and the TA-MMP-2 complex were 14.87 ± 0.08 and 15.07 ± 0.07 , respectively, and those for the free MMP-9 and the TA-MMP-9 complex were 14.58 ± 0.05 and

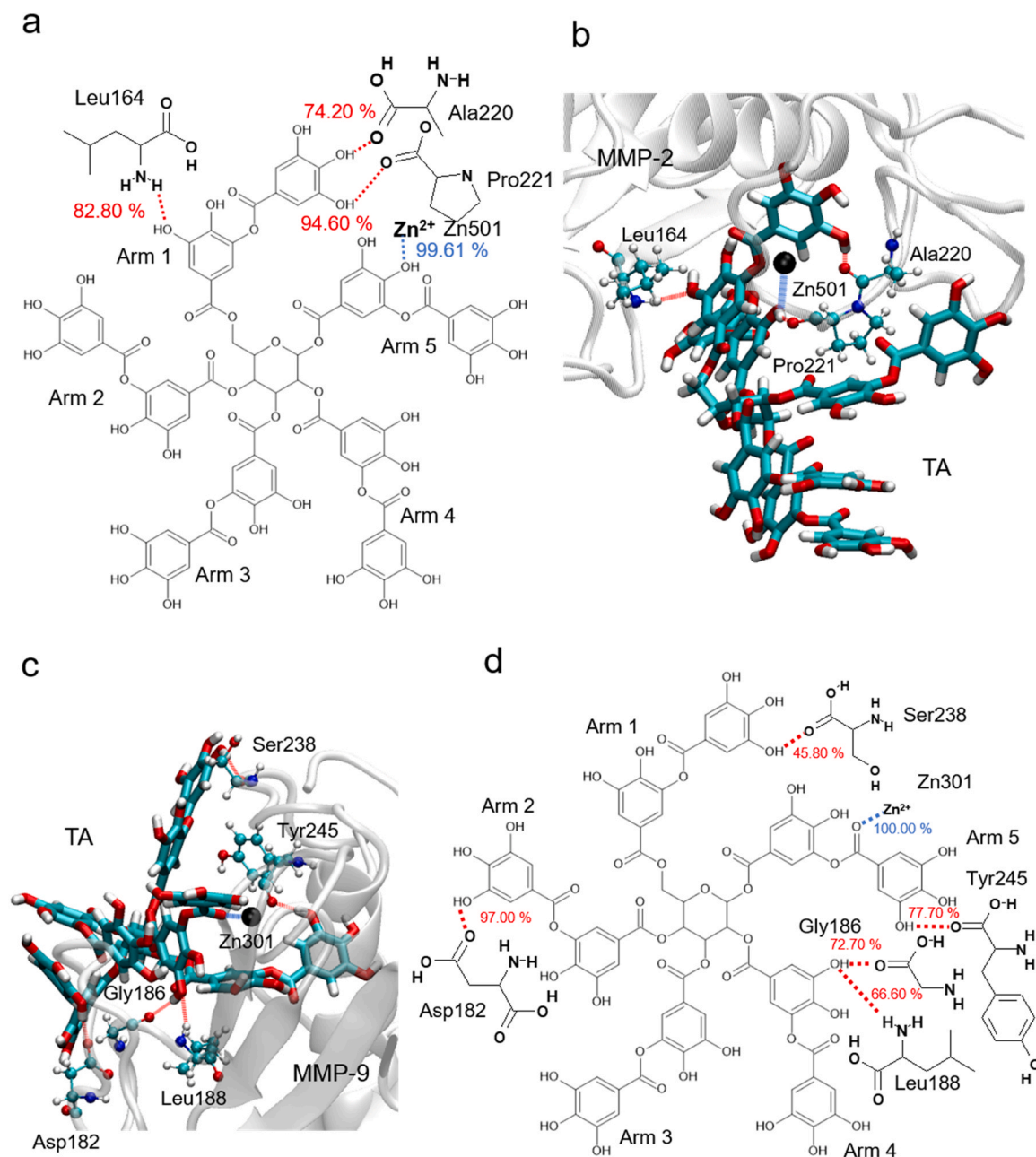


Fig. 3. (a) 2D interaction plots of the TA–MMP-2 complex. (b) Equilibrated binding structures in the MD simulation of the TA–MMP-2 complex. (c) Equilibrated binding structures in the MD simulation of the TA–MMP-9 complex. (d) 2D interaction plots of the TA–MMP-9 complex. Hydrogen bonds between TA and both MMPs with occupancies higher than 40% and metal–organic coordination bonds between TA and catalytic zinc ions are highlighted. Red lines represent intermolecular hydrogen bonds. Blue lines represent metal–organic coordination bonds. Individual occupancies for hydrogen bonds and metal–organic coordination bonds are also labeled in (a) and (d). In (b) and (c), carbon, oxygen, nitrogen, hydrogen, and zinc atoms are plotted in cyan, red, blue, white, and black, respectively.

14.73 ± 0.05 , respectively. TA binding with both MMPs caused RMSD and Rg to increase only slightly, indicating that binding may not cause large structural changes. The above fluctuations in RMSD and Rg values were low, indicating that the protein structures of both MMPs were stable during the MD simulation. A structural comparison of the free MMP and the two TA–MMP complexes is shown in Fig. 6(c) and (d). The molecular structure of the two TA–MMP complexes shared a high similarity with the structures of the two free MMPs. Previous experimental studies have shown that the binding of TA on scaffolds made from collagen and MMPs helps transform the random coil into a β -sheet and thereby stabilize the

structure of the scaffold [50]. However, our results indicated that the binding of TA did not cause an obvious conformational change in either MMP. Detailed secondary structure comparison in Fig. S1 also showed no large secondary structure change between the two free MMPs and the two TA–MMP complexes.

Fig. 7(a) and (b) show the root mean square fluctuations (RMSF) of $C\alpha$ atoms as a function of residue number for both MMPs to analyze protein flexibility [51]. All residue numbers were re-numbered from 1 for two reasons. 1. The residue Gly190A was inserted after Lys190, and residues 224–226 were removed in 1QIB [33]. 2. We aligned 1QIB and 5112 for clarity. As expected, the large

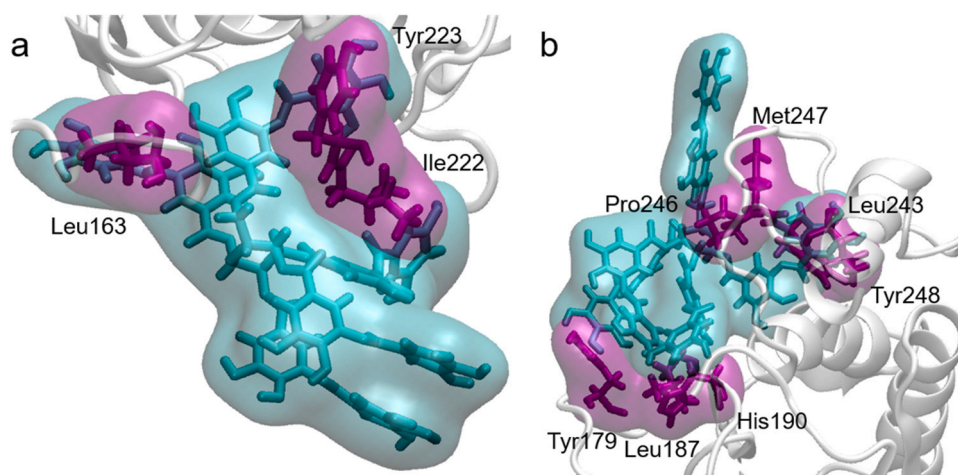


Fig. 4. Molecular structure of the (a) TA–MMP-2 complex and (b) TA–MMP-9 complex with the hydrophobic interactions highlighted. TA is represented in cyan, and residues are represented in purple. Hydrophobic interactions are represented by a surface with the same color as the TA or the residues.

fluctuations were located in loop structures. Important binding sites from [Tables S3 and S4](#) are labeled. Most of these binding sites had lower RMSF values than other regions, indicating that TA binds with both MMPs at the rigid regions. Thus, TA bound stably to both MMPs. Overall, TA mainly bound to the MMPs at two regions: residues 163–164 and 134–137 for MMP-2 and residues 179–190 and 126–136 for MMP-9.

We compared the binding locations of residues between the two MMPs. The results are shown in [Table S5](#). For hydrogen bonding

residues, TA bound with both MMPs at the same residue locations, such as Leu164 and Ala220 for MMP-2 and Leu188 and Tyr245 for MMP-9. MMP-2 had one different binding residue, Pro221, and MMP-9 had three different binding residues, Asp182, Gly186, and Ser238. TA formed hydrophobic interactions with both MMPs at the same residue locations, such as Leu163, Ile222, and Tyr223 for MMP-2 and Leu187, Met247, and Tyr248 for MMP-9. MMP-2 had no additional binding residues, and MMP-9 had four additional binding residues, Tyr179, His190, Leu243, and Pro246. MMP-9 had more

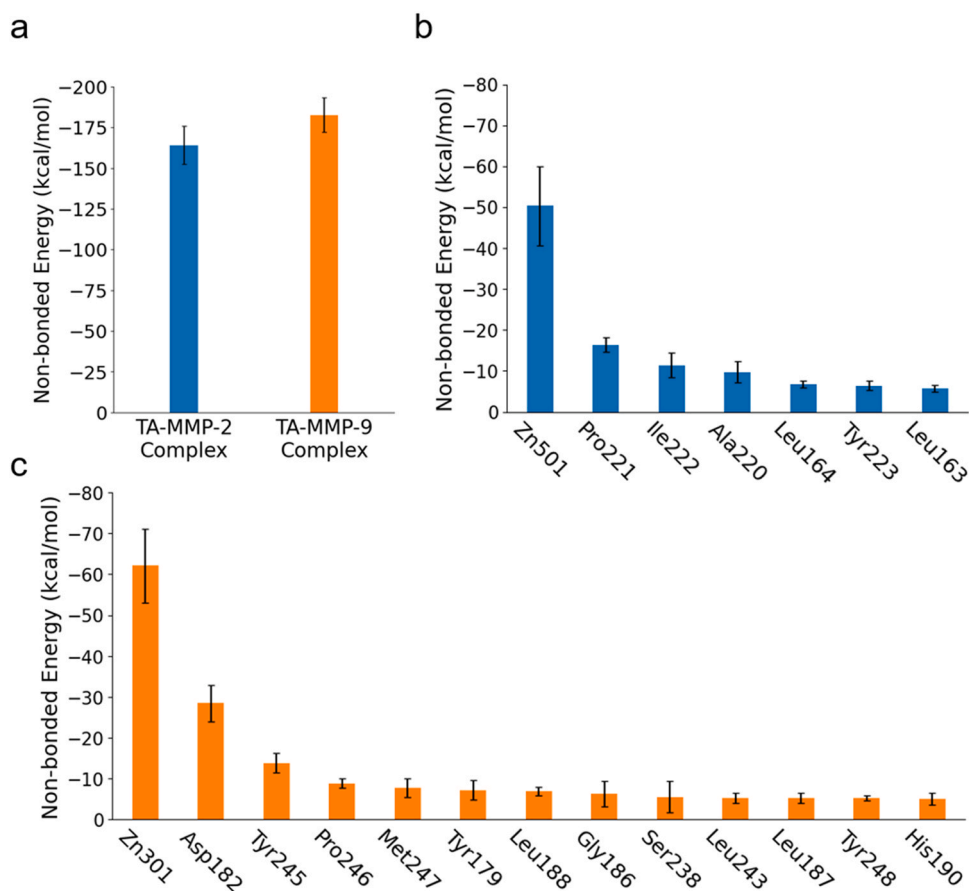


Fig. 5. (a) Total nonbonded energy for both TA–MMP complexes. Decomposition of nonbonded energy for the (b) TA–MMP-2 complex and (c) TA–MMP-9 complex.

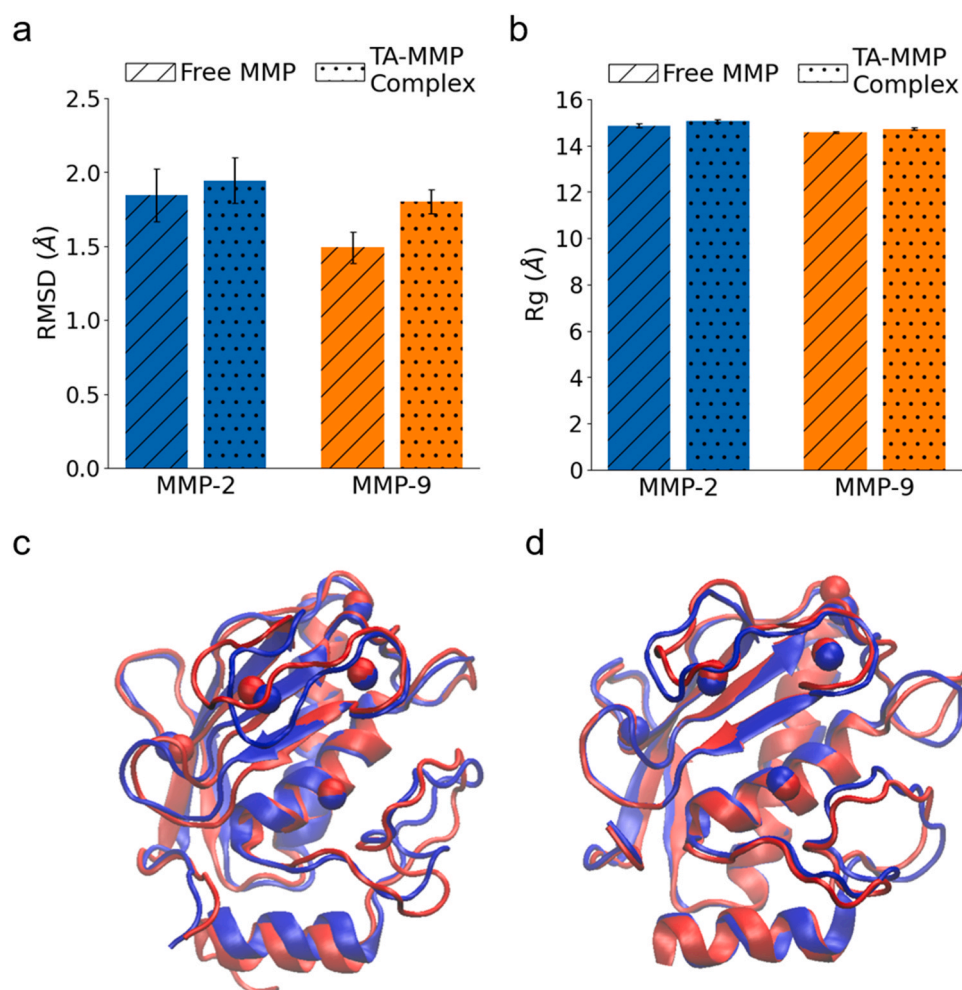


Fig. 6. (a) RMSD values of both free MMPs and TA–MMP complexes. (b) Rg values of both free MMPs and TA–MMP complexes. (c) Structure comparison of free MMP-2 and the TA–MMP-2 complex. (d) Structure comparison of free MMP-9 and the TA–MMP-9 complex. The structures of the free MMPs and TA–MMP complexes are shown in blue and red, respectively.

hydrogen bonding and hydrophobic residues than MMP-2, indicating that MMP-9 interacted more strongly than MMP-2 with TA. Our docking results regarding the binding site of TA are compatible with those of a previous study on other MMP inhibitors (MMPis), such as GA [30] and zinc-binding groups (ZBGs) [52]. Moreover, specific residues of MMPs that form H-bonds with TA, such as Leu164 and Pro221 for MMP-2 and Leu188 for MMP-9, also form H-bonds with some other MMPis [30,52]. This finding sheds further light on selective inhibitors, showing that they should not only interact with zinc but also bind to a number of specific residues.

In Fig. 7(a), some regions had larger differences in RMSF values between the TA–MMP-2 complex and free MMP-2, such as LsV-hB, LhB-hC, and hC, indicating that binding may increase the flexibility of these regions. In Fig. 7(b), only the LsV-hB region had a larger RMSF value difference between the TA–MMP-9 complex and free MMP-9.

The enzymatic inhibition of MMP-2/–9 with TA has been confirmed by zymography assay but is not yet understood on a molecular level [30]. The hypothesis is that the gallate residue plays a key role in the interaction of TA with MMP [30], and in our simulations, this suggestion is confirmed – strong hydrogen bonds form between the digallic acid arm and MMP-2/–9. We further compared the

molecular interactions of TA and gallic acid (GA), both relatively small phenolic chemicals, with MMP-2 and MMP-9. A previous study showed that GA inhibited the proteolytic activity of MMP-2 and MMP-9 [53]. In their docking simulations, two GA molecules were considered, and the results showed that the GA molecules formed hydrogen bonds with MMP-2 and MMP-9. Two GA molecules can be treated as two pyrogallol groups in the two digallic acid arms of TA. Thus, our results are consistent with previous results [53] in showing that the binding mode involved multiple digallic acid arms in both MMP-2 and MMP-9. Because of its five digallic acid arms, TA exhibits additional possible binding sites that could strengthen its interactions with MMPs.

Our results show differences in binding interactions and mechanisms between the TA–MMP-2 and TA–MMP-9 complexes. These differences might lead to a stronger inhibitory effect of TA on MMP-9 protein and further have a more prolonged effect on the inhibition of MMP-9 activity and the related biological functions; for example, MMP-9 is involved in keratinocyte migration and granulation tissue remodeling [22]. Our study provides a deeper understanding of the molecular structures and interactions of TA with these two MMPs, which could potentially be extended to the design of a multi-functional TA-based hydrogel.

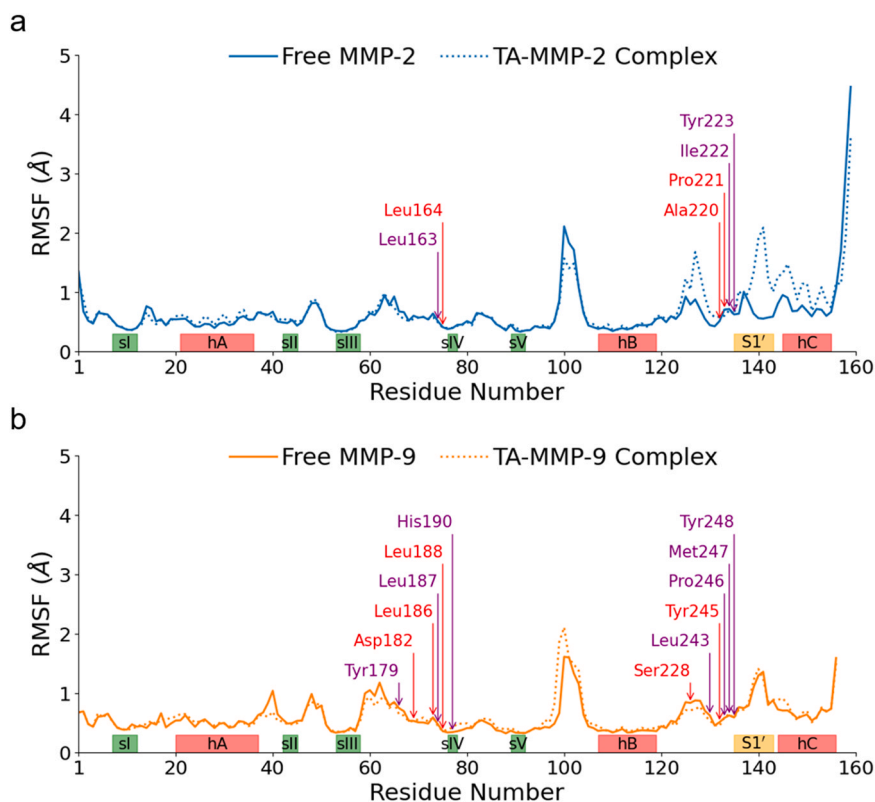


Fig. 7. (a) RMSF of free MMP-2 and the TA-MMP-2 complex. (b) RMSF of free MMP-9 and the TA-MMP-9 complex. Key residues obtained from Tables S3 and S4 and secondary structures obtained from PDB files are also labeled in the figure. Residues related to hydrogen bonding and hydrophobic interactions are colored in red and purple, respectively.

4. Conclusions

The present study examined the binding mechanism and binding structures of TA-MMP-2 and TA-MMP-9 complexes through full atomistic simulations. The molecular binding structures of the TA-MMP-2 and TA-MMP-9 complexes were obtained from molecular docking and molecular dynamics simulations. TA mainly bound to the MMPs at two regions (residues 134–137 and 163–164 for MMP-2 and residues 126–136 and 179–190 for MMP-9) through hydrogen bonds, metal-organic coordination bonds and hydrophobic interactions. TA formed hydrogen bonds with MMP-2 through two digallic acid arms and with MMP-9 through four digallic acid arms, resulting in stronger nonbonded interactions in the TA-MMP-9 complex than in the TA-MMP-2 complex. Furthermore, RMSF analysis revealed that most of the binding sites were in rigid regions, indicating stable binding of the TA-MMP-2 and TA-MMP-9 complexes. A fundamental understanding of the binding mechanism of TA-MMP complexes at the molecular scale could potentially be applied in the development of new biomaterials and biomedicine.

CRedit authorship contribution statement

Ya-Tang Chiang: Data curation, Formal analysis, Writing – original draft. **Yu-Bai Xiao:** Formal analysis, Visualization, Revising the manuscript. **Shan-hui Hsu:** Conceptualization, Writing – review & editing, Supervision. **Shu-Wei Chang:** Conceptualization, Hardware, Writing – review & editing, Supervision. **Chia-Ching Chou:** Conceptualization, Hardware, Writing – review & editing, Supervision.

Conflicts of Interest

The authors declare no conflict of interest.

Acknowledgments

This work was supported by the National Science and Technology Council, Taiwan (111-2636-E-002-022, 111-2221-E-002-171-MY2 and 112-2636-E-002-004), and the National Taiwan University (111L891903).

Appendix A. Supporting information

Supplementary data associated with this article can be found in the online version at [doi:10.1016/j.csbj.2023.04.011](https://doi.org/10.1016/j.csbj.2023.04.011).

References

- [1] Cao H, et al. Current hydrogel advances in physicochemical and biological response-driven biomedical application diversity. *Signal Transduct Target Ther* 2021;6(1):1–31.
- [2] Cruz-Acuna R, García AJ. Synthetic hydrogels mimicking basement membrane matrices to promote cell-matrix interactions. *Matrix Biol* 2017;57:324–33.
- [3] Kopeček J. Hydrogel biomaterials: a smart future? *Biomaterials* 2007;28(34):5185–92.
- [4] Kopeček J, Yang J. Smart self-assembled hybrid hydrogel biomaterials. *Angew Chem Int Ed* 2012;51(30):7396–417.
- [5] Caló E, Khutoryanskiy VV. Biomedical applications of hydrogels: a review of patents and commercial products. *Eur Polym J* 2015;65:252–67.
- [6] Chen Y, et al. Bio-inspired hydrogels with fibrous structure: a review on design and biomedical applications. *Biomater Adv* 2022;212799.
- [7] Shoukat H, et al. Hydrogels as potential drug-delivery systems: network design and applications. *Ther Deliv* 2021;12(5):375–96.
- [8] Asadi N, et al. Multifunctional hydrogels for wound healing: special focus on biomacromolecular based hydrogels. *Int J Biol Macromol* 2021;170:728–50.
- [9] Vedadghavami A, et al. Manufacturing of hydrogel biomaterials with controlled mechanical properties for tissue engineering applications. *Acta Biomater* 2017;62:42–63.
- [10] Baldwin A, Booth BW. Biomedical applications of tannic acid. *J Biomater Appl* 2022;36(8):1503–23.
- [11] Kaczmarek B. Tannic acid with antiviral and antibacterial activity as a promising component of biomaterials—A minireview. *Materials* 2020;13(14):3224.
- [12] Lu R, et al. Medical applications based on supramolecular self-assembled materials from tannic acid. *Front Chem* 2020;8:583484.

- [13] Shi W, et al. Tannic acid-inspired, self-healing, and dual stimuli responsive dynamic hydrogel with potent antibacterial and anti-oxidative properties. *J Mater Chem B* 2021;9(35):7182–95.
- [14] Okamoto Y, et al. Effects of phosphoric acid and tannic acid on dentine collagen. *J Oral Rehabil* 1991;18(6):507–12.
- [15] Velmurugan P, et al. Investigation on interaction of tannic acid with type I collagen and its effect on thermal, enzymatic, and conformational stability for tissue engineering applications. *Biopolymers* 2014;101(5):471–83.
- [16] Bedran-Russo A, et al. Mechanical properties of tannic-acid-treated dentin matrix. *J Dent Res* 2009;88(9):807–11.
- [17] Farias D, Miguez PA, Swift Jr EJ. Cross-linkers and the Dentin Matrix. *J Esthet Restor Dent* 2014;26(1):72–6.
- [18] Kong W, et al. Tannic acid induces dentin biomaterialization by crosslinking and surface modification. *RSC Adv* 2022;12(6):3454–64.
- [19] Daré RG, et al. Tannic acid, a promising anti-photoaging agent: Evidences of its antioxidant and anti-wrinkle potentials, and its ability to prevent photodamage and MMP-1 expression in L929 fibroblasts exposed to UVB. *Free Radic Biol Med* 2020;160:342–55.
- [20] Nakkala JR, et al. Immunomodulatory biomaterials and their application in therapies for chronic inflammation-related diseases. *Acta Biomater* 2021;123:1–30.
- [21] Nissinen L, Kähäri V-M. Matrix metalloproteinases in inflammation. *Biochim Et Biophys Acta (BBA)-Gen Subj* 2014;1840(8):2571–80.
- [22] Salo T, et al. Expression of matrix metalloproteinase-2 and -9 during early human wound healing. *Lab Investig; a J Tech Methods Pathol* 1994;70(2):176–82.
- [23] Li K, Tay FR, Yiu CKY. The past, present and future perspectives of matrix metalloproteinase inhibitors. *Pharmacol Ther* 2020;207:107465.
- [24] Xue M, Le NT, Jackson CJ. Targeting matrix metalloproteinases to improve cutaneous wound healing. *Expert Opin Ther Targets* 2006;10(1):143–55.
- [25] Cabral-Pacheco GA, et al. The roles of matrix metalloproteinases and their inhibitors in human diseases. *Int J Mol Sci* 2020;21(24):9739.
- [26] Tombulturk FK, et al. Regulation of MMP 2 and MMP 9 expressions modulated by AP-1 (c-jun) in wound healing: improving role of *Lucilia sericata* in diabetic rats. *Acta Diabetol* 2019;56(2):177–86.
- [27] Li Y, et al. Construction of multifunctional hydrogel based on the tannic acid-metal coating decorated MoS₂ dual nanozyme for bacteria-infected wound healing. *Bioact Mater* 2022;9:461–74.
- [28] Pan W, et al. Facile formation of injectable quaternized chitosan/tannic acid hydrogels with antibacterial and ROS scavenging capabilities for diabetic wound healing. *Int J Biol Macromol* 2022;195:190–7.
- [29] Sahiner N, et al. Biocompatible and biodegradable poly (Tannic Acid) hydrogel with antimicrobial and antioxidant properties. *Int J Biol Macromol* 2016;82:150–9.
- [30] Zhang H, et al. Intramyocardial injection of tannic acid attenuates postinfarction remodeling: a novel approach to stabilize the breaking extracellular matrix. *J Thorac Cardiovasc Surg* 2009;137(1):216–22. e2.
- [31] Zhou H, et al. Tannic Acid-A Universal Immobilization and Fixation Agent for Nanocarbon Materials: a novel strategy for aqueous fabrication of functional nanocarbon coating onto silicon-based substances. *ACS Sustain Chem Eng* 2019;7(22):18534–41.
- [32] Malde AK, et al. An automated force field topology builder (ATB) and repository: version 1.0. *J Chem Theory Comput* 2011;7(12):4026–37.
- [33] Dhanaraj V, et al. X-ray structure of gelatinase A catalytic domain complexed with a hydroxamate inhibitor. *Croat Chem Acta* 1999;72(2–3):575–91.
- [34] Nuti E, et al. Sugar-Based Arylsulfonamide Carboxylates as Selective and Water-Soluble Matrix Metalloproteinase-12 Inhibitors. *ChemMedChem* 2016;11(15):1626–37.
- [35] Overall CM, Kleinfeld O. Towards third generation matrix metalloproteinase inhibitors for cancer therapy. *Br J Cancer* 2006;94(7):941–6.
- [36] Trott O, Olson AJ. AutoDock Vina: improving the speed and accuracy of docking with a new scoring function, efficient optimization, and multithreading. *J Comput Chem* 2010;31(2):455–61.
- [37] Santos EMS, et al. Gallic acid modulates phenotypic behavior and gene expression in oral squamous cell carcinoma cells by interfering with leptin pathway. *Pathol-Res Pract* 2018;214(1):30–7.
- [38] Huey R, Morris GM, Forli S. Using AutoDock 4 and AutoDock vina with AutoDockTools: a tutorial. *Scripps Res Inst Mol Graph Lab* 2012;10550:92037.
- [39] Bello M, Hasan MK. Elucidation of the inhibitory activity of plant-derived SARS-CoV inhibitors and their potential as SARS-CoV-2 inhibitors. *J Biomol Struct Dyn* 2021;1–13.
- [40] Singh T, Adekoya OA, Jayaram B. Understanding the binding of inhibitors of matrix metalloproteinases by molecular docking, quantum mechanical calculations, molecular dynamics simulations, and a MMGBSA/MMBAppI study. *Mol Biosyst* 2015;11(4):1041–51.
- [41] Phillips JC, et al. Scalable molecular dynamics with NAMD. *J Comput Chem* 2005;26(16):1781–802.
- [42] Huang J, et al. CHARMM36m: an improved force field for folded and intrinsically disordered proteins. *Nat Methods* 2017;14(1):71–3.
- [43] Kim, S, et al., CHARMM-GUI ligand reader and modeler for CHARMM force field generation of small molecules. 2017, Wiley Online Library.
- [44] Prada-Gracia D, Shevchuk R, Rao F. The quest for self-consistency in hydrogen bond definitions. *J Chem Phys* 2013;139(8):084501.
- [45] Fu Y, Zhao J, Chen Z. Insights into the molecular mechanisms of protein-ligand interactions by molecular docking and molecular dynamics simulation: A case of oligopeptide binding protein. *Comput Math Methods Med* 2018;2018.
- [46] MacKerell Jr AD, et al. All-atom empirical potential for molecular modeling and dynamics studies of proteins. *J Phys Chem B* 1998;102(18):3586–616.
- [47] Paramashivam S, Dhiraviam KN. Computational insights into the identification of a potent matrix metalloproteinase inhibitor from *Indigofera aspalathoides* to control cancer metastasis. *3 Biotech* 2021;11:1–19.
- [48] Kufareva I, Abagyan R. Methods of protein structure comparison. *Homology modeling*. Springer; 2011. p. 231–57.
- [49] Lobanov MY, Bogatyreva N, Galzitskaya O. Radius of gyration as an indicator of protein structure compactness. *Mol Biol* 2008;42(4):623–8.
- [50] Li Y, et al. Tannic acid/Sr²⁺-coated silk/graphene oxide-based meniscus scaffold with anti-inflammatory and anti-ROS functions for cartilage protection and delaying osteoarthritis. *Acta Biomater* 2021;126:119–31.
- [51] Bornot A, Etchebest C, De Brevern AG. Predicting protein flexibility through the prediction of local structures. *Protein: Struct, Funct, Bioinforma* 2011;79(3):839–52.
- [52] Giustiniano M, et al. Amino acid derivatives as new zinc binding groups for the design of selective matrix metalloproteinase inhibitors. *J Amino Acids* 2013;2013.
- [53] Filipiak K, et al. Dietary gallic acid and anthocyanin cytotoxicity on human fibrosarcoma HT1080 cells. A study on the mode of action. *Food Funct* 2014;5(2):381–9.